



Cite this: *EES Catal.*, 2024, 2, 1228

## Salt precipitation and water flooding intrinsic to electrocatalytic $\text{CO}_2$ reduction in acidic membrane electrode assemblies: fundamentals and remedies

Qianqian Bai,<sup>†[a](#)</sup> Likun Xiong,<sup>†[b](#)</sup> Yongjia Zhang,<sup>a</sup> Mutian Ma,<sup>a</sup> Zhenyang Jiao,<sup>a</sup> Fenglei Lyu,  <sup>\*[ac](#)</sup> Zhao Deng  <sup>\*[ac](#)</sup> and Yang Peng  <sup>\*[ac](#)</sup>

Renewable electricity powered electrocatalytic  $\text{CO}_2$  reduction ( $\text{eCO}_2\text{R}$ ) is an emerging carbon-negative technology that upgrades  $\text{CO}_2$  into valuable chemicals and simultaneously stores intermittent renewable energy.  $\text{eCO}_2\text{R}$  in anion exchange membrane (AEM)-based membrane electrode assemblies (MEAs) has witnessed high faradaic efficiency (FE). But severe  $\text{CO}_2$  crossover in AEMs results in low  $\text{CO}_2$  single-pass conversion ( $\text{SPC}_{\text{CO}_2}$ ) and burdens the energy-intensive  $\text{CO}_2$  separation process. Utilizing cation exchange membranes (CEMs) and acidic anolytes,  $\text{eCO}_2\text{R}$  in acidic MEAs is capable of addressing the  $\text{CO}_2$  crossover issue and overcoming the  $\text{SPC}_{\text{CO}_2}$  limits in their AEM counterparts. Alkali metal cations such as  $\text{K}^+/\text{Cs}^+$  are always adopted in acidic MEAs to suppress the competing hydrogen evolution reaction (HER) and boost  $\text{eCO}_2\text{R}$  kinetics. However,  $\text{K}^+/\text{Cs}^+$  accumulates and precipitates in the form of carbonate/bicarbonate salts in the cathode, which accelerates water flooding, deteriorates the gas-electrode–electrolyte interface, and limits the durability of acidic  $\text{eCO}_2\text{R}$  MEAs to a few hours. In this mini-review, we discuss the fundamentals of salt precipitation and water flooding and propose potential remedies including inhibiting  $\text{K}^+/\text{Cs}^+$  accumulation, decreasing local  $\text{CO}_3^{2-}/\text{HCO}_3^-$  concentration, and water management in gas diffusion electrodes (GDEs). We hope that this mini-review will spur more insightful solutions to address the salt precipitation and water flooding issues and push acidic  $\text{eCO}_2\text{R}$  MEAs toward industrial implementations.

Received 20th August 2024,  
Accepted 3rd September 2024

DOI: 10.1039/d4ey00170b

[rsc.li/eescatalysis](http://rsc.li/eescatalysis)

### Broader context

Electrocatalytic  $\text{CO}_2$  reduction ( $\text{eCO}_2\text{R}$ ) represents an emerging carbon-negative technology for the production of valuable chemicals from  $\text{CO}_2$ ,  $\text{H}_2\text{O}$ , and renewable electricity. Benefiting from short  $\text{CO}_2$  diffusion length ( $\sim 50$  nm),  $\text{CO}_2$  electrolysis in membrane electrode assemblies (MEAs) based on gas diffusion electrodes (GDEs) greatly boosts up the current density of  $\text{eCO}_2\text{R}$ . MEAs utilizing anion exchange membranes (AEMs) have attained high  $\text{eCO}_2\text{R}$  faradaic efficiency, but suffer from severe  $\text{CO}_2$  crossover and low carbon utilization efficiency ( $\leq 50\%$ ), which burdens the energy-intensive  $\text{CO}_2$  separation process. Utilizing cation exchange membranes (CEMs) and acidic electrolytes, acidic  $\text{eCO}_2\text{R}$  MEAs address the  $\text{CO}_2$  crossover issue. However, alkali cations such as  $\text{K}^+$  and  $\text{Cs}^+$  are adopted to suppress the competing hydrogen evolution reaction (HER) and boost the  $\text{eCO}_2\text{R}$  kinetics, which causes severe salt precipitation and water flooding and seriously limits the durability of acidic MEAs to a few hours. Herein, we discuss the fundamentals of salt precipitation and water flooding in acidic  $\text{eCO}_2\text{R}$  MEAs and propose remedies that potentially overcome these issues, including mitigating/eliminating  $\text{K}^+/\text{Cs}^+$  accumulation, reducing local  $\text{CO}_3^{2-}/\text{HCO}_3^-$  concentration, and innovating the GDE structure. This mini-review may spur more inspiration to address salt precipitation and water flooding issues in acidic  $\text{eCO}_2\text{R}$  MEAs.

## 1. Introduction

Electrocatalytic  $\text{CO}_2$  reduction ( $\text{eCO}_2\text{R}$ ) driven by renewable electricity from sunlight and wind holds great promise to upcycle  $\text{CO}_2$  into valuable chemicals and simultaneously store intermittent renewable energy into chemical bonds.<sup>1–3</sup> In virtue of the high energy efficiency, high production rate as well as feasible scalability at the industrial scale,  $\text{CO}_2$  electrolysis in

<sup>a</sup> *Soochow Institute for Energy and Material Innovations, College of Energy, Soochow University, Suzhou 215006, P. R. China. E-mail: fllv@suda.edu.cn, ypeng@suda.edu.cn*

<sup>b</sup> *School of Chemical and Environmental Engineering, Shanghai Institute of Technology, Shanghai, 201418, China*

<sup>c</sup> *Jiangsu Key Laboratory for Advanced Negative Carbon Technologies, Soochow University, Suzhou 215123, China*

† These authors contributed equally to this work.



zero-gap membrane electrode assemblies (MEAs) based on gas diffusion electrodes (GDEs) has drawn great attention.<sup>4-8</sup> Benefiting from the much shorter CO<sub>2</sub> diffusion length in GDEs (~50 nm) than that in conventional H-type cells (~50  $\mu\text{m}$ ),<sup>9</sup> industrially relevant current densities ( $\geq 200 \text{ mA cm}^{-2}$ ) with appreciable faradaic efficiencies (>90% for CO and >80% for C<sub>2</sub>H<sub>4</sub>) have been attained in CO<sub>2</sub> MEAs utilizing anion exchange membranes (AEMs) and neutral anolytes (*e.g.* aqueous KHCO<sub>3</sub>/CsHCO<sub>3</sub> solution).<sup>10,11</sup> However, severe CO<sub>2</sub> loss ( $\geq 50\%$ ) brought by carbonate/bicarbonate (CO<sub>3</sub><sup>2-</sup>/HCO<sub>3</sub><sup>-</sup>) crossover in AEMs remains a significant challenge. As a result, the theoretical limits of the CO<sub>2</sub> single-pass conversion (SPC<sub>CO<sub>2</sub></sub>) in AEM-based MEAs are merely 50% for CO and 25% for C<sub>2</sub>H<sub>4</sub>, which seriously burdens the energy-intensive CO<sub>2</sub> separation and purification process.<sup>12</sup>

Conventional CO<sub>2</sub> capture consumes energy from 170 to 390 kJ mol<sub>CO<sub>2</sub></sub><sup>-1</sup> depending on the CO<sub>2</sub> source, which translates into a voltage loss of 0.88 V caused by CO<sub>2</sub> recapture from the anode even with minimum energy consumption of 170 kJ mol<sup>-1</sup> and 100% faradaic efficiency.<sup>13-15</sup> The energy penalty caused by anode CO<sub>2</sub> recapture for C<sub>2</sub>H<sub>4</sub> is ~1.55 times that of the C<sub>2</sub>H<sub>4</sub> Gibbs free energy of reaction even with the maximum 25% SPC<sub>CO<sub>2</sub></sub>, which makes the neutral MEAs untenable.<sup>16</sup> Though techno-economic assessments demonstrate that the industrially relevant benchmarks of SPC<sub>CO<sub>2</sub></sub> are 30% for C<sub>1</sub> and 15% for C<sub>2</sub> products with CO<sub>2</sub> crossover, the same model also shows an apparent cost reduction if no CO<sub>2</sub> crossover exists.<sup>17</sup> Therefore, it is imperative to solve the CO<sub>2</sub> crossover issue to eliminate the energy cost for anode CO<sub>2</sub> recapture. It is also noteworthy that SPC<sub>CO<sub>2</sub></sub> should not be the only target for eCO<sub>2</sub>R MEAs. 100% SPC<sub>CO<sub>2</sub></sub> may not be required since such high SPC<sub>CO<sub>2</sub></sub> brings additional issues of competing HER under the low CO<sub>2</sub> available conditions.<sup>16,18</sup> Maximizing the concentration of targeted eCO<sub>2</sub>R products in the cathode downstream, *i.e.*, maximizing SPC<sub>CO<sub>2</sub></sub> without sacrificing the eCO<sub>2</sub>R selectivity, is a more reasonable and practical merit.<sup>19</sup>

eCO<sub>2</sub>R MEAs utilizing cation exchange membranes (CEMs) and acidic anolytes, namely acidic MEAs, are capable of addressing the CO<sub>2</sub> crossover issue and potentially overcoming the theoretical SPC<sub>CO<sub>2</sub></sub> limit in neutral MEAs. In acidic MEAs, CO<sub>3</sub><sup>2-</sup>/HCO<sub>3</sub><sup>-</sup> from the cathode catalyst layer (CL) reacts with H<sup>+</sup> from the CEM and generates CO<sub>2</sub> and H<sub>2</sub>O at the CL/CEM interface, eliminating the CO<sub>2</sub> crossover to the anode.<sup>20</sup>

In zero-gap eCO<sub>2</sub>R MEAs, the cathode, ion exchange membrane, and anode are intimately assembled. The ion mobility of transported ionic species and ionic conductivity of the membrane dominate the ohmic loss between the cathode and anode. In acidic eCO<sub>2</sub>R MEAs, H<sup>+</sup> exhibits much higher ionic mobility ( $3.62 \times 10^{-7} \text{ m}^2 \text{ s}^{-1} \text{ V}^{-1}$ ) than CO<sub>3</sub><sup>2-</sup> ( $7.46 \times 10^{-8} \text{ m}^2 \text{ s}^{-1} \text{ V}^{-1}$ ) in neutral eCO<sub>2</sub>R MEAs, rendering low ohmic loss in the ion exchange membrane and high energy efficiency.<sup>21</sup> More importantly, the commercially available perfluorosulfonic acid-based CEMs with high ionic conductivity and long-term stability have been widely adopted in proton exchange membrane fuel cells and water electrolyzers, which paves the way for the industrial implementation of acidic eCO<sub>2</sub>R MEAs.

The proton source for eCO<sub>2</sub>R in acidic MEAs is H<sub>2</sub>O. While the proton source for the hydrogen evolution reaction (HER) is H<sub>3</sub>O<sup>+</sup> under low overpotential and H<sub>2</sub>O under high overpotential. In acidic eCO<sub>2</sub>R MEAs with abundant H<sub>3</sub>O<sup>+</sup>, the Tafel step (\*H + \*H = H<sub>2</sub> + 2\*) or Heyrovsky (\*H + H<sup>+</sup> + e<sup>-</sup> = H<sub>2</sub> + \*) step is usually the rate-determining step for the HER with low overpotential, which shows fast kinetics with a low Tafel slope (30 mV dec<sup>-1</sup> for Tafel step and 39 mV dec<sup>-1</sup> for Heyrovsky step).<sup>22</sup> In contrast, the activation of CO<sub>2</sub> into \*CO<sub>2</sub><sup>-</sup> is both kinetically sluggish with a Tafel slope of 118 mV dec<sup>-1</sup>, and thermodynamically unfavorable. Moreover, the low CO<sub>2</sub> solubility (~34 mM) and high H<sub>3</sub>O<sup>+</sup> accessibility in acidic electrolytes make the CO<sub>2</sub> adsorption on the surface of conventional metallic eCO<sub>2</sub>R catalysts very difficult.<sup>23,24</sup> The fast kinetics of the competing HER in the H<sup>+</sup>-rich microenvironment therefore leads to low eCO<sub>2</sub>R selectivity in acidic MEAs.<sup>25</sup>

In order to suppress the HER, alkali cations such as K<sup>+</sup>/Cs<sup>+</sup> are added into the acidic electrolyte, in which they play a key role in modulating the eCO<sub>2</sub>R and HER kinetics (Fig. 1).<sup>26</sup> Partially desolvated alkali cations stabilize the \*CO<sub>2</sub><sup>-</sup> intermediates *via* short range electrostatic interaction and medium range electric field-dipole interaction. The direct coordination in M<sup>+</sup>-O(CO<sub>2</sub>) also enhances the charge transfer to the CO<sub>2</sub> unit.<sup>25</sup> Alkali cations accumulated in the outer Helmholtz plane (OHP) modify the distribution of the electric field in the double layer and suppress the migration of H<sub>3</sub>O<sup>+</sup>.<sup>27</sup> Moreover, OH<sup>-</sup> produced during eCO<sub>2</sub>R (eqn (1)) neutralizes the H<sub>3</sub>O<sup>+</sup>. Therefore, local high pH can be generated when the formation rate of OH<sup>-</sup> compensates the migration of H<sub>3</sub>O<sup>+</sup>.<sup>28</sup> The alkali cations also play a key role in C-C bond formation. Partially desolvated alkali cations coordinate with \*CO + \*CO in the double layer, stabilize the key \*OCCO intermediates and lower the energy barrier for C-C bond formation.<sup>29,30</sup> Meanwhile, alkali cations induce a hydrophobic microenvironment, which tunes the structure of interfacial water and favors the C-C coupling.<sup>31,32</sup>

In acidic eCO<sub>2</sub>R MEAs, K<sup>+</sup>/Cs<sup>+</sup> is usually added to the anolytes. K<sup>+</sup>/Cs<sup>+</sup> is continuously dragged across the CEMs *via* the electric field and accumulates at the cathode CL, then combines with locally generated CO<sub>3</sub><sup>2-</sup>/HCO<sub>3</sub><sup>-</sup>, and forms

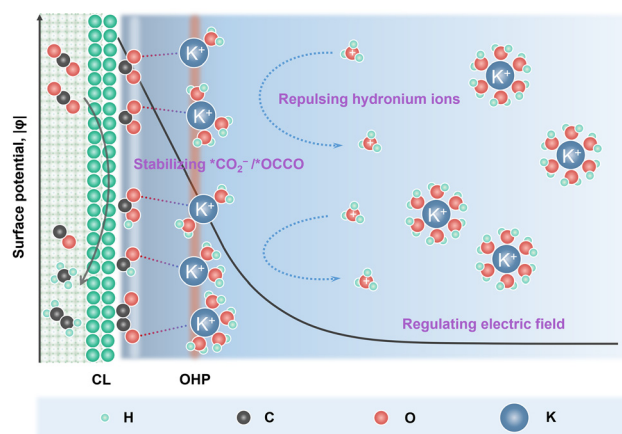


Fig. 1 Schematic illustration of the alkali cation effects in acidic eCO<sub>2</sub>R.



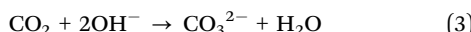
carbonate/bicarbonate salt precipitation. Salt precipitation destroys the hydrophobicity of GDEs and leads to severe water flooding, which not only blocks the transportation of gaseous  $\text{CO}_2$ , but also deteriorates the gas–catalyst–electrolyte interface and eventually causes MEA failure.<sup>33</sup>

In this mini-review, we will discuss the origins of salt precipitation and water flooding in acidic  $\text{eCO}_2\text{R}$  MEAs from a fundamental viewpoint. Then, we will summarize remedies that potentially overcome salt precipitation and water flooding issues, including mitigating/eliminating  $\text{K}^+/\text{Cs}^+$  accumulation, reducing local  $\text{CO}_3^{2-}/\text{HCO}_3^-$  concentration, and innovating the structure of GDEs. Perspectives on how to elevate the durability,  $\text{SPC}_{\text{CO}_2}$  and energy efficiency of acidic  $\text{eCO}_2\text{R}$  MEAs through the catalyst, ionomer, membrane and their interface engineering will be discussed in the end. We hope that this mini-review will enlighten more insightful thoughts in this field and push  $\text{eCO}_2\text{R}$  in acidic MEAs toward industrial implementations.

## 2. Fundamentals of salt precipitation and water flooding in acidic $\text{eCO}_2\text{R}$ MEAs

### 2.1. Salt precipitation in acidic $\text{eCO}_2\text{R}$ MEAs

Alkali cations such as  $\text{K}^+/\text{Cs}^+$  are capable of stabilizing the key  $^{*}\text{CO}_2^-$  intermediates *via* electrostatic interaction and retard the  $\text{H}_3\text{O}^+$  diffusion kinetics through the electric field effect, thus promoting  $\text{eCO}_2\text{R}$  reactivity and suppressing the HER in acid.<sup>25</sup> Since CEMs are conductive to  $\text{K}^+/\text{Cs}^+$ , plenty of  $\text{K}^+/\text{Cs}^+$  from the anolyte is continuously transported across the CEMs *via* electroosmosis and accumulates at the cathode. Owing to the generation of  $\text{OH}^-$  in  $\text{eCO}_2\text{R}$  (eqn (1)) and the suppressed  $\text{H}_3\text{O}^+$  diffusion, the surface of cathode CL can be highly alkaline although bulk anolyte is acidic.  $\text{CO}_2$  is chemically absorbed in the  $\text{OH}^-$ -rich layer and transformed into  $\text{HCO}_3^-$  and  $\text{CO}_3^{2-}$  (eqn (2) and (3)).



As shown in Fig. 2, the combination of  $\text{K}^+/\text{Cs}^+$  and  $\text{CO}_3^{2-}/\text{HCO}_3^-$  generates  $\text{K}_2\text{CO}_3/\text{Cs}_2\text{CO}_3$  or  $\text{KHCO}_3/\text{CsHCO}_3$  salts, which precipitate in the microporous layer when their concentration exceeds the solubility limits (2.24 M for  $\text{KHCO}_3$ , 3.49 M for  $\text{CsHCO}_3$ , 7.93 M for  $\text{K}_2\text{CO}_3$ , and 8.01 M for  $\text{Cs}_2\text{CO}_3$  at 20 °C in pure  $\text{H}_2\text{O}$ ).<sup>33</sup> These porous and hydrophilic carbonate/bicarbonate salts accelerate electrolyte penetration into the GDEs, consequently speeding up the water flooding process. The salt precipitation strongly depends on the type and concentration of alkali cations, and the net flux of water ( $J_{\text{H}_2\text{O},\text{net}}$ ) in the cathode (eqn (4)). Carbonate/bicarbonate salts with higher solubility, low cation concentration in the anolyte, and low ion mobility have slower precipitation rates. Assuming that there is no crossover of anionic species such as  $\text{HCO}_3^-/\text{CO}_3^{2-}$ , the  $J_{\text{H}_2\text{O},\text{net}}$  is determined by the diffusion ( $J_{\text{diff}}$ ) from the anode to the cathode driven by concentration gradients, the electro-osmotic drag ( $J_{\text{eod}}$ ) caused

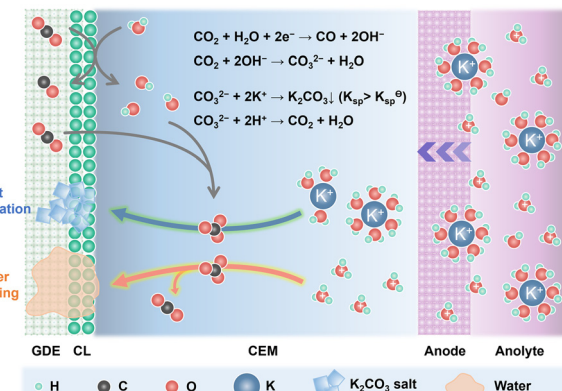


Fig. 2 Schematic illustration of the salt precipitation and water flooding process in acidic  $\text{eCO}_2\text{R}$  MEAs.

by solvated alkali cations and  $\text{H}_3\text{O}^+$  from anode to cathode, the consumption of  $\text{eCO}_2\text{R}$  ( $J_{\text{con}}$ ), and the back convection ( $J_{\text{bc}}$ ) due to the repellence by the hydrophobic cathode GDE.<sup>34</sup>

$$J_{\text{H}_2\text{O},\text{net}} = J_{\text{diff}} + J_{\text{eod}} - J_{\text{con}} - J_{\text{bc}} \quad (4)$$

$J_{\text{H}_2\text{O},\text{net}}$  is dominated by the interplay of the CEM, cathode GDE, and operational current density. CEMs with low water uptake have low  $J_{\text{diff}}$  and  $J_{\text{eod}}$ . Operating at low current density and using solvated cations with low mobility decreases the  $J_{\text{eod}}$  and  $J_{\text{con}}$ . Using cathode GDEs with high hydrophobicity and CEMs with low thickness favors the  $J_{\text{bc}}$ .

### 2.2. Water flooding in acidic $\text{eCO}_2\text{R}$ MEAs

Water flooding in GDEs remains a critical challenge in acidic  $\text{eCO}_2\text{R}$  MEAs since it blocks the transportation of  $\text{CO}_2$  to the surface of catalysts and results in severe HER. Central to this issue is the gas/liquid flow scenario in porous structures. Assuming the GDE as a porous matrix with interconnected cylindrical pores (Fig. 3a–c), liquid transport in the GDE is driven by the capillary differential pressure ( $\Delta P$ ) between gas pressure ( $P_g$ ) and liquid pressure ( $P_l$ ), as shown in eqn (5) derived from the Young–Laplace equation.

$$\Delta P = P_g - P_l = \frac{2\gamma^1 \cos \alpha}{r} \quad (5)$$

where  $\gamma^1$  is the surface tension of the liquid,  $\alpha$  is the contact angle, and  $r$  is the pore radius.

Wetting dynamics at the interface, defined by the contact angle between the solid surface and the liquid droplets, can be categorized into the Cassie, the Cassie–Wenzel coexistence, and the Wenzel state (Fig. 3d–f). Each state delineates a unique pathway for  $\text{CO}_2$  transportation through the GDE, corresponding to distinct flow patterns including flow-through ( $\Delta P > 2\gamma^1/r$ ), flow-by ( $-2\gamma^1/r \leq \Delta P \leq 2\gamma^1/r$ ), and GDE flooding ( $\Delta P < -2\gamma^1/r$ ).

$\Delta P$  is dynamically influenced by the high  $\text{H}_2\text{O}$  flux from the anolyte to cathode GDE, which increases the  $P_l$ . In addition to  $\text{H}_2\text{O}$  diffusion from the anolyte,  $\text{H}_2\text{O}$  flux to the cathode GDE is



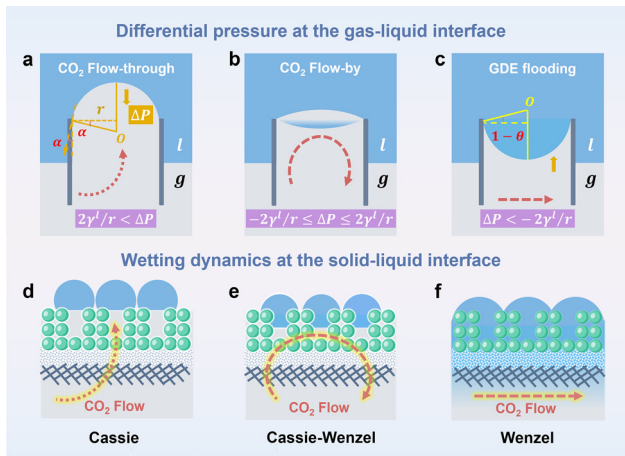


**Fig. 3** Schematic illustration of differential pressure at the gas–liquid interface and corresponding (a)  $\text{CO}_2$  flow-through, (b)  $\text{CO}_2$  flow-by and (c) GDE flooding modes. Wetting dynamics at the solid–liquid interface including (d) Cassie state, (e) Cassie–Wenzel coexistence state, and (f) Wenzel state.

amplified *via* the electroosmosis of  $\text{H}^+$  and  $\text{K}^+/\text{Cs}^+$  in an acidic MEA because  $\text{H}^+$  and  $\text{K}^+/\text{Cs}^+$  transfer is always in conjunction with the hydrated shells, *i.e.*  $\text{H}_3\text{O}^+$  and  $\text{K}(\text{H}_2\text{O})_m^+/\text{Cs}(\text{H}_2\text{O})_m^+$ . Additionally, excessive  $\text{H}_2\text{O}$  is generated at the CL/CEM interface during the regeneration of  $\text{CO}_2$  from  $\text{HCO}_3^-$  and  $\text{CO}_3^{2-}$  (eqn (6) and (7)).

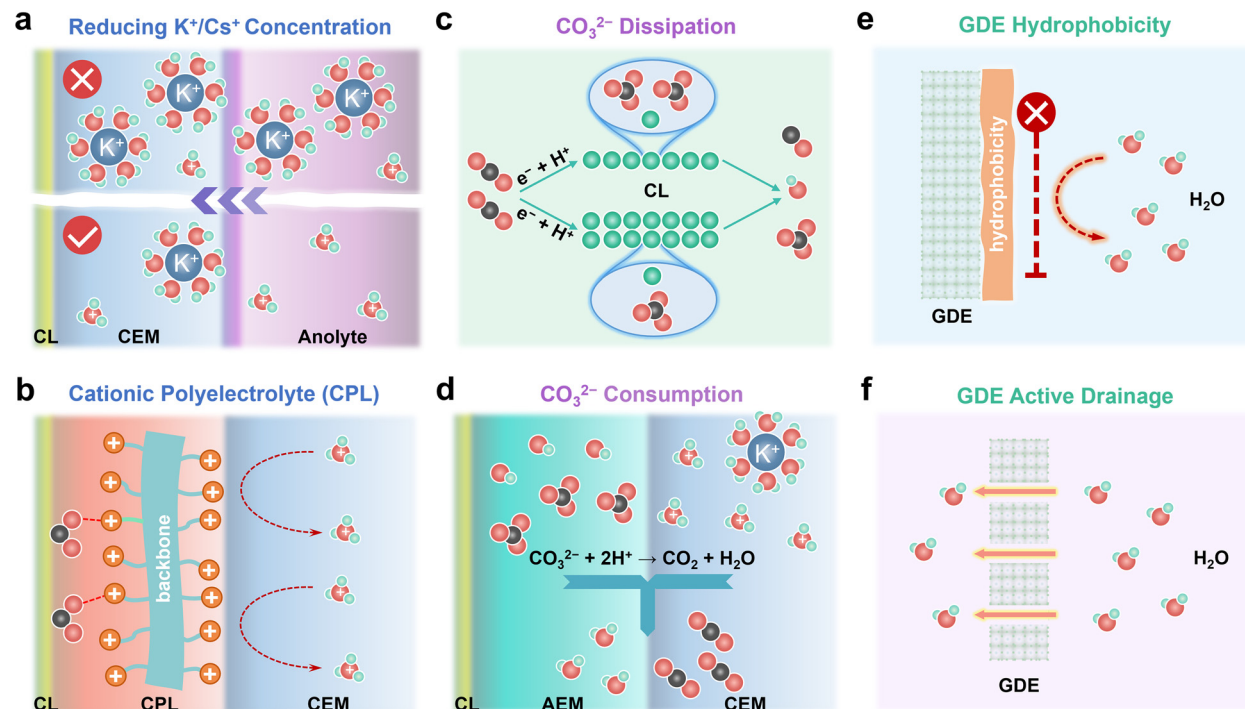
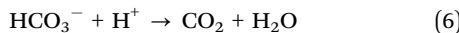
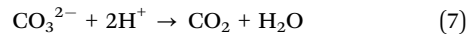


**Fig. 4** Remedies of mitigating salt precipitation and water flooding in acidic eCO<sub>2</sub>R MEAs including (a) reducing  $\text{K}^+/\text{Cs}^+$  concentration in anolytes, (b) replacing  $\text{K}^+/\text{Cs}^+$  with a cationic polyelectrolyte layer (CPL), (c)  $\text{CO}_3^{2-}$  dissipation in the catalyst layer (CL), (d) accelerating  $\text{CO}_3^{2-}$  consumption, (e) tailoring GDE hydrophobicity, and (f) GDE active drainage.



Moreover, the imbalance between  $\text{CO}_2$  consumption and gas production rates at the interface, electrowetting, degradation of GDE hydrophobicity, and salt precipitation also contribute to the hydrostatic/hydrodynamic differential pressure by changing the  $P_g$ ,  $\gamma$ <sup>1</sup> and  $\alpha$ .<sup>35</sup> Such variations in the pressure balance can gradually reduce  $\Delta P$  below the critical transition threshold, causing the CEM system to shift from the flow-by model to the GDE flooding model. We note that the triphasic gas–electrode–electrolyte interface under operando conditions is much more complicated. For example, gases are generated at the catalyst/liquid interface due to the Joule heating. The differential pressure might vary strongly among different parts due to the complex catalyst/hydrophobic moiety/carbon interface.

### 3. Remedies for salt precipitation and water flooding in acidic eCO<sub>2</sub>R MEAs

Salt precipitation and water flooding are always intertwined together, which severely deteriorates the gas–electrode–electrolyte interface and poses obstacles to the stability of acidic eCO<sub>2</sub>R MEAs. The accumulation of  $\text{K}^+/\text{Cs}^+$ , *in situ* formation of high-concentration  $\text{CO}_3^{2-}/\text{HCO}_3^-$  on the cathode CL, and high  $\text{H}_2\text{O}$  flux from the anolyte are the main culprits for severe salt precipitation and water flooding in acidic eCO<sub>2</sub>R MEAs. In this section, remedies including  $\text{K}^+/\text{Cs}^+$ ,  $\text{CO}_3^{2-}/\text{HCO}_3^-$ , and  $\text{H}_2\text{O}$  management (Fig. 4) *via* engineering the electrodes,



electrolyte, and membrane are proposed to mitigate these issues and enhance the durability of acidic MEAs.

### 3.1. Preventing $K^+/Cs^+$ accumulation or replacing $K^+/Cs^+$ with cationic polyelectrolytes

$K^+/Cs^+$  accumulated in the CL and microporous layer supplies cations for salt precipitation. Therefore, preventing  $K^+/Cs^+$  accumulation represents a proactive solution to alleviate salt precipitation in acidic MEAs. Generally, the less  $K^+/Cs^+$  migrates across the CEM, the longer the time for salts to precipitate. Reducing the concentration of  $K^+/Cs^+$  in the anolyte is a straightforward way to limit the quantity of  $K^+/Cs^+$  that electro-migrates from the anolyte to the cathode. In an ideal case, the concentration of  $K^+/Cs^+$  in the anolyte should be as low as possible on the premise of high  $eCO_2R$  selectivity (Fig. 4a). By doing so, the salt precipitation kinetics are effectively decelerated. Generalized modified Poisson–Nernst–Planck (GMPNP) modeling demonstrates that the concentration of cations ( $C_{M^+}$ ) and the identity of  $M^+$  affect  $eCO_2R$  by tuning the electric field strength in the stern layer. Increasing the  $C_{M^+}$  and adding cations with smaller solvated sizes such as  $K^+$  and  $Cs^+$  results in higher partial current density ( $j_{CO}$ ). Meanwhile, the mass transport of  $H^+$  is inhibited when  $C_{M^+}$  is not less than  $C_{H^+}$ . Decreasing the  $C_{K^+}$  from 0.8 M to 0.02 M suppresses the  $KHCO_3$  precipitation in the acidic flow cell at 200  $mA\ cm^{-2}$ , but also leads to a low  $FE_{CO}$ .<sup>36</sup> These results match with the report from Pan *et al.*<sup>18</sup> In their work, the influence of  $Cs^+$  and  $H^+$  concentration in the anolyte on the  $j_{CO}$  and faradaic efficiency of CO ( $FE_{CO}$ ) using Ag/PTFE as the cathode GDE in acidic MEAs is systematically studied. Diluted anolyte (0.01 M  $H_2SO_4$  + 0.01 M  $Cs_2SO_4$ ) is optimal for high  $FE_{CO}$  (~80%) at low current density (60  $mA\ cm^{-2}$ ). While low pH and  $Cs^+$  concentration (0.2 M  $H_2SO_4$  + 0.01 M  $Cs_2SO_4$ ) are more favorable for  $FE_{CO}$  (75%) at high current density (140  $mA\ cm^{-2}$ ). By using 0.01 M  $H_2SO_4$  + 0.01 M  $Cs_2SO_4$  as anolyte, 50-hour stability at 60  $mA\ cm^{-2}$  with ~90%  $SPC_{CO_2}$  and 80%  $FE_{CO}$  is achieved. In a recent work, Kamiya *et al.* performed a quantitative analysis of how the transported alkali cations regulate the  $eCO_2R$  selectivity in MEAs and suggested that continuously supplying a high amount of  $K^+$  is not necessary for  $C_{2+}$  formation.<sup>37</sup> Intermittently supplying concentrated  $KHCO_3$  is able to extend the durability of MEAs by alleviating the salt precipitation, which provides an effective method to prevent  $K^+/Cs^+$  accumulation.

Salt precipitation and water flooding can be mitigated but not eliminated as long as alkali cations exist in anolytes. During continuous operation in acidic MEAs, anolyte pH gradually decreases because metal cation accumulation at cathode inhibits  $H^+$  transportation across CEMs and further induces  $H^+$  accumulation in the anolytes. Such imbalanced ion transportation also causes the unstable operation of acidic MEAs. Operating acidic  $eCO_2R$  MEAs with pure acid or even pure water as anolytes potentially overcomes instability issues brought by imbalanced ion transportation and rapid salt precipitation. Recently, Dich *et al.* reported the using of pure water as the anolyte and periodically injecting  $Cs^+$  containing solution into the cathode

chamber to provide cations for  $CO_2$  activation in a forward-bias bipolar membrane (f-BPM) with a porous anion exchange layer (AEL).<sup>38</sup> A long stability of 200 hours at 100  $mA\ cm^{-2}$  with  $FE_{CO}$  ~80% is achieved because cation accumulation is prohibited by using pure water as the anolyte. The use of porous AEL for recovered  $CO_2$  recirculation in conjunction with CEMs also enables a maximum  $SPC_{CO_2}$  of 52%.

Apart from using alkali cations, weakly coordinating organic cations, such as water-soluble tetraalkylammonium cations (PDDA), are intrinsically capable of supporting  $eCO_2R$  on Au and Ag on par with alkali cations.<sup>39</sup> Based on the modified Poisson–Boltzmann model, the electric field strength generated by the immobilized benzimidazole cationic group (CG) is in the same order as that generated by  $K^+$ ,<sup>40</sup> which allows Cu to reach 80%  $C_{2+}$  in a pure acid electrolyte without  $K^+$  and to operate stably for 150 h. Therefore, a cationic polyelectrolyte layer (CPL) with sufficiently high charge density sandwiched between the cathode CL and the CEM is also capable of modulating the electrical field and stabilizing  $*CO_2^-$  as  $K^+/Cs^+$  does (Fig. 4b).<sup>41</sup>

Polyelectrolytes with a high charge density usually have high solubility in water, which induces instability of the cathode CL/CPL/CEM interface because the water flux from the anode is increased during  $CO_2$  recovery (eqn (6) and (7)). To mitigate the loss of polyelectrolytes, Fan *et al.* demonstrated that immobilizing poly(diallyldimethylammonium) (PDDA) on graphene oxide (GO) *via* electrostatic interaction could displace metal cations for acidic  $eCO_2R$  MEAs with pure acid or even pure water as the anolyte.<sup>42</sup> A 50-hour stability at 100  $mA\ cm^{-2}$  with a  $FE_{CO}$  of about 70% is demonstrated in the MEA fed with 0.01 M  $H_2SO_4$ . A  $FE_{CO}$  of 78% with an energy efficiency of 30% could be achieved using a PDDA-GO modified Ag catalyst at 100  $mA\ cm^{-2}$  and 40 °C.

The key role of CPLs is activating  $CO_2$  without alkali cations, transporting  $CO_3^{2-}$  and recovered  $CO_2$ , and providing a local alkaline environment by suppressing the migration of  $H_3O^+$ . First, CPLs should have high ion exchange capacity (IEC) and maximize ionic conductivity, which favors  $CO_2$  activation and  $CO_3^{2-}$  transportation. Second, CPLs should have moderate water uptake to manage the water content in the cathode CL since the low water uptake will cause water starvation in the cathode GDE and high water uptake will cause GDE flooding and fast  $H_3O^+$  migration. Third, CPLs should have high mechanical and chemical stability, which not only can withstand both local acid and alkaline environments but also can mechanically stabilize the cathode CL/CPL/CEM interface. Fourth, CPLs should be permeable for gaseous  $CO_2$ , which favors transporting recovered  $CO_2$  back to the cathode CL.

The knowledge gained from AEMs and anion exchange ionomers (AEIs) can be transferred to speed up the development of CPLs. Decent reviews on AEMs and AEIs<sup>43–46</sup> have summarized the desired properties, such as  $OH^-$  conductivity (60–100  $mS\ cm^{-1}$ ), IEC (>1.5  $meq\ g^{-1}$ ), tensile strain (20 MPa), and water uptake (50–80%), which can provide instructive knowledge for CPLs.<sup>45</sup> In CPLs, cationic groups such as quaternary ammonium, pyrrolidonium, piperidinium and imidazolium groups are generally integrated into the mainchain or



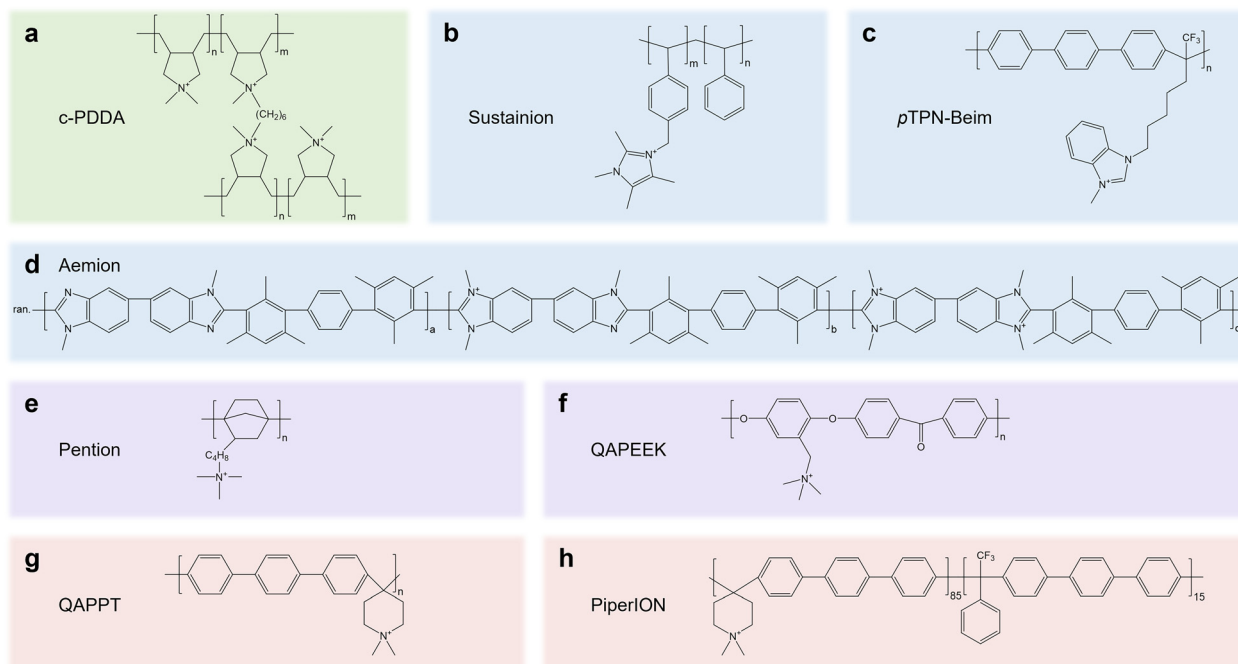


Fig. 5 Molecular structures of AEMs/AEIs that are feasible in  $\text{eCO}_2\text{R}$  electrolyzers fed with pure acid or pure water, including (a) c-PDDA, (b) Sustainion, (c) pTPN-Beim, (d) Aemion, (e) Pention, (f) QAPEEK, (g) QAPPT and (h) PiperION.

side chain of polymer backbones such as polystyrene, polybenzylimidazole, poly terphenyl, and polynorbornene. We summarize the molecular structure of AEMs/AEIs (Fig. 5) that have been proven to be feasible in pure water/pure acid-fed acidic  $\text{eCO}_2\text{R}$  electrolyzers (c-PDDA, Sustainion, Aemion, and Piperion)<sup>16,47–49</sup> or pure water fed neutral  $\text{eCO}_2\text{R}$  MEAs (pTPN-Beim, Pention, QAPEEK, and QAPPT),<sup>10,50–52</sup> which may guide the design of high-performance CPLs in the future.

### 3.2. Reducing local $\text{CO}_3^{2-}/\text{HCO}_3^-$ concentration by dissipation or rapid consumption

Reducing local  $\text{CO}_3^{2-}/\text{HCO}_3^-$  concentration is also an important direction to decelerate salt precipitation kinetics since salt precipitation occurs only when the critical concentrations of metal cations and  $\text{CO}_3^{2-}/\text{HCO}_3^-$  are achieved. Dissipation and rapid consumption present promising tactics to reduce the local  $\text{CO}_3^{2-}/\text{HCO}_3^-$  concentration.

As illustrated in eqn (1)–(3), local  $\text{CO}_3^{2-}/\text{HCO}_3^-$  concentration strongly depends on the faradaic current at the cathode GDE. Increasing the amount of active site enabled by increasing the CL thickness or the density of the active site reduces the faradaic current generated per active site, thus reducing the local  $\text{OH}^-$  generated per active site (Fig. 4c).<sup>53</sup> In such a dissipation strategy,  $\text{CO}_3^{2-}/\text{HCO}_3^-$  is kept at low concentrations. It should be noted that  $\text{CO}_2$  and ion transportation is slowed down when the CL is too thick. Therefore, the CL thickness should be subtly balanced. Mass-transport modelling shows that the local  $\text{CO}_2$  concentration depends on the CL thickness, porosity and operating current densities.<sup>9,54</sup> Increasing the CL thickness from 1  $\mu\text{m}$  to 5  $\mu\text{m}$  decreases the local  $\text{CO}_2$  concentration from 20 mM to 17 mM at

100  $\text{mA cm}^{-2}$ . The local  $\text{CO}_2$  concentration reduced from 17 mM to 10 mM with CL thickness of 5  $\mu\text{m}$  when the current density rises from 100  $\text{mA cm}^{-2}$  to 300  $\text{mA cm}^{-2}$ .<sup>55</sup> Increasing the CL porosity enhances the gas permeability and facilitates the gas transport. Increasing the CL porosity from 0.3 to 0.7 improves the current density by more than 100  $\text{mA cm}^{-2}$  in a wetted CL.<sup>56</sup>

In the electric double layer (EDL),  $\text{CO}_2$ ,  $\text{HCO}_3^-$  and  $\text{CO}_3^{2-}$  are in equilibrium. According to Henry's law, increasing input  $\text{CO}_2$  pressure ( $P_{\text{CO}_2}$ ) results in increased  $\text{CO}_{2(\text{eq})}$ , which tunes the  $\text{CO}_{2(\text{eq})}-\text{CO}_3^{2-}-\text{HCO}_3^-$  equilibrium and potentially decreases the local  $\text{CO}_3^{2-}/\text{HCO}_3^-$  concentration. Moreover, increasing  $P_{\text{CO}_2}$  is also capable of boosting the  $\text{eCO}_2\text{R}$  kinetics and suppressing the competing HER by enhancing the local  $\text{CO}_2$  concentration.<sup>57</sup> When the same mole of  $\text{CO}_2$  is fed, higher  $\text{CO}_2$  pressure will increase the  $\text{SPC}_{\text{CO}_2}$ . However, if  $\text{CO}_2$  availability is not the limiting factor, increasing the  $\text{CO}_2$  pressure will not increase the  $\text{SPC}_{\text{CO}_2}$  instead.

Rapid consumption of the  $\text{CO}_3^{2-}/\text{HCO}_3^-$  generated in the CL represents another important solution to reduce the local  $\text{CO}_3^{2-}/\text{HCO}_3^-$  concentration (Fig. 4d). In a f-BPM MEA, the regeneration of  $\text{CO}_2$  occurs at the AEM/CEM interface, where  $\text{CO}_3^{2-}/\text{HCO}_3^-$  from the AEM is consumed by  $\text{H}^+$  from the CEM. Therefore, accelerating the transportation rate of  $\text{CO}_3^{2-}/\text{HCO}_3^-$  from the CL to the AEM/CEM interface and enlarging the AEM/CEM interface potentially increases the consumption rate of  $\text{CO}_3^{2-}/\text{HCO}_3^-$ , thereby decreasing the local  $\text{CO}_3^{2-}/\text{HCO}_3^-$  in CL. In practice, this strategy can be achieved by constructing the intimate CL/AEM/CEM interface by the catalyst-coated membrane (CCM) and direct membrane deposition (DMD) method,<sup>58</sup> which also has another benefit of reducing the



transportation resistance of ions and increasing the overall energy efficiency.

### 3.3. Managing $\text{H}_2\text{O}$ content in cathode GDEs by surface hydrophobicity and active drainage

Salt precipitation and water flooding are generally trapped into a vicious cycle and finally block the  $\text{CO}_2$  transportation in GDEs. Though the salt precipitation problem can be potentially solved by Remedies 3.1 and 3.2, water flooding still exists because of the *in situ* formation of  $\text{H}_2\text{O}$  during  $\text{CO}_2$  regeneration (eqn (6) and (7)). On the other hand,  $\text{H}_2\text{O}$  plays a critical role as the proton source for  $\text{eCO}_2\text{R}$ . Therefore, managing  $\text{H}_2\text{O}$  content in cathode GDEs, which can be realized by tailoring surface hydrophobicity or actively draining, is significant to balance the selectivity and stability of the acidic  $\text{eCO}_2\text{R}$  MEAs.

The cathode GDE provides spaces for uniformly distributing  $\text{CO}_2$ ,  $\text{H}_2\text{O}$ , and electrons. However, the transport pathways for  $\text{CO}_2$  and  $\text{H}_2\text{O}$  are usually intertwined, which impedes  $\text{CO}_2$  diffusion. Hydrophobic treatment of the GDE is therefore essential to decouple  $\text{CO}_2$  and  $\text{H}_2\text{O}$  transportation (Fig. 4e). In previous work, Wang *et al.* reported a hydrophobized integral GDE embedding undercoordinated Ni–N–C active sites (NiNF) for full-pH  $\text{CO}_2$  electroreduction in MEAs.<sup>59</sup> By virtue of the integral architecture, hierarchical porosity, and high hydrophobicity, it not only enhances  $\text{CO}_2$  transportation but also mitigates salt precipitation and water flooding. NiNF exhibits a near-unity faradaic efficiency of CO and stable operation for more than 273 hours in neutral MEAs and a high single-pass  $\text{CO}_2$  conversion of 78% in acidic MEAs. Post-mortem characterizations reveal that the failure of MEAs is mainly attributed to the loss of hydrophobicity.

Conventional GDEs are composed of macroporous carbon fiber paper (CFP), microporous layer (MPL), and CL, among which micropores in the MPL are the most easily flooded due to electrochemical wetting by water. Active draining by innovating the GDE structure holds promise to enhance its tolerance to water flooding and extend its durability (Fig. 4f). For example, through tailoring the wettability gradient and introducing large-size pores by laser drilling in a Janus carbon-based GDE, water spontaneously transports from the hydrophobic side to hydrophilic side, enabling a remarkable antiflooding capability.<sup>60</sup> In addition to conventional carbon-based GDEs, metal foam-based GDEs have recently drawn great attention because of the high conductivity of the metal foam and abundant large pores with microns in size. A hydrophobic catalytic layer can be *in situ* grown on metal foams through etching metal foams or electrodeposition.<sup>11,61</sup> Such architecture not only enables a high  $\text{CO}_2$  diffusion rate by surface hydrophobicity but also enhances resilience to flooding because the large pores are favorable for drainage, offering great opportunities to mitigate GDE flooding.

In Remedy 3.1, reducing the concentration of  $\text{K}^+/\text{Cs}^+$  helps to extend the stability of acidic MEAs and simultaneously utilizes the cation effect to keep the high  $\text{eCO}_2\text{R}$  selectivity. However, the salt precipitation after long-term operation is unavoidable since the CEMs are permeable to  $\text{K}^+/\text{Cs}^+$ . Utilizing a CPL to

replace  $\text{K}^+/\text{Cs}^+$  can eliminate the salt precipitation issue. But how to rationally fabricate the CPL with high chemical and mechanical robustness, and stabilize the cathode CL/CPL/CEM interface still remains to be explored. In Remedy 3.2, increasing the CL thickness or the density of active sites can reduce the local concentration of  $\text{CO}_3^{2-}$ , but will cause the problem of slow  $\text{CO}_2$  and ion transfer. Constructing an intimate cathode CL/AEM/CEM interface by the CCM or DMD method can boost the  $\text{CO}_3^{2-}$  transfer and consumption, and increase the energy efficiency at the same time. The flux of  $\text{H}^+$ ,  $\text{CO}_3^{2-}$ , and  $\text{CO}_2$  should be carefully balanced at the CL/AEM/CEM interface. In Remedy 3.3, increasing the hydrophobicity of GDEs can facilitate  $\text{CO}_2$  transportation and increase the resistance to water flooding. But the loss of hydrophobicity by electrowetting and loss of PTFE binder over time cannot be avoided. The active drainage of GDEs can effectively manage water content in GDEs. More efforts should be devoted to properly engineering the distribution of wettable areas since the flooding behavior and water distribution in cathode GDEs remain elusive, which may increase the fabrication of the GDEs. In addition, periodically adding cations or refreshing the anode electrolyte is necessary to compensate for the loss of cations brought by the water flow out of the electrolyte.

We note that some of these strategies including reducing the concentration of  $\text{K}^+/\text{Cs}^+$ , tailoring the porosity and thickness of cathode CL, constructing a cathode CL/membrane interface for favorable ion transfer, increasing the hydrophobicity or constructing wettable area for water management in the cathode GDE can be extended to the neutral/alkaline  $\text{eCO}_2\text{R}$  MEA too. But the optimal conditions in these strategies vary since neutral/alkaline  $\text{eCO}_2\text{R}$  MEAs manifest different local environments (such as local  $\text{CO}_2$  concentration and local pH) from acidic MEAs. The AEIs of neutral/alkaline  $\text{eCO}_2\text{R}$  are critical for managing the  $\text{CO}_2$  gas and  $\text{CO}_3^{2-}$  ion transfer in the cathode CL. But the CPLs in acidic  $\text{eCO}_2\text{R}$  MEAs should be more challenging since they not only provide the gas and ion transfer pathway but also are capable of stabilizing the cathode CL/CPL/CEM interface during  $\text{CO}_2$  recovery.

## 4. Summary and perspective

Acidic MEAs have become an important direction in the development of  $\text{eCO}_2\text{R}$  for industrial applications because of their high carbon utilization and energy efficiency. However, the durability issue of acidic  $\text{eCO}_2\text{R}$  MEAs brought by salt precipitation and water flooding remains challenging. In this minireview, we discuss the origins of salt precipitation and water flooding from the fundamental viewpoint and propose potential remedies including inhibiting  $\text{K}^+/\text{Cs}^+$  accumulation, decreasing local  $\text{CO}_3^{2-}/\text{HCO}_3^-$ , and water management in GDEs.

Apart from the electrode, electrolyte, and membrane engineering, recovery steps/washing is necessary to recover the performance loss caused by salt precipitation and water flooding with relatively low operation cost. For example, washing the cathode GDE with water can dissolve the salt precipitates and



maintain the moderate  $\text{FE}_{\text{CO}}$  (85%) during continuous electrolysis.<sup>62</sup> Periodically activating and regenerating the cathode GDE with cation containing solution (1 M CsOH in 1:3 isopropanol/water mixture) in the pure water-fed electrolyzer can maintain the stability for 200 h.<sup>38,63</sup> In addition to the commonly used aqueous electrolyte, organic electrolyte can also be utilized to reduce the carbonation of aqueous electrolyte. By utilizing dimethyl sulfoxide as the solvent and acetic acid/acetate as the proton source in the aprotic solvent-based  $\text{eCO}_2\text{R}$  system, Chu *et al.* demonstrated that attenuating the water content in an organic medium and using a nonnucleophilic buffer with a matched pKa simultaneously mitigates carbonation and the HER.<sup>64</sup>

Although progress has been made to address the salt precipitation and water flooding to extend the durability of acidic  $\text{eCO}_2\text{R}$  MEAs, there is still a long way ahead to meet the requirements for stability (5 years), energy efficiency ( $\sim 50\%$ ), and  $\text{SPC}_{\text{CO}_2}$  (30% and 15% for  $\text{C}_1$  and  $\text{C}_2$  products) according to the techno-economic assessment.<sup>17</sup> To push acidic  $\text{eCO}_2\text{R}$  MEAs toward large-scale implementation, research efforts also should be devoted to the following fields:

(1) Fabricating selective and stable  $\text{eCO}_2\text{R}$  electrocatalysts for acidic MEAs. Some heterogeneous molecular electrocatalysts are intrinsically active and selective for acidic  $\text{eCO}_2\text{R}$  in a pure water-fed BPM electrolyzer, which completely eliminates the salt precipitation issue. For example, the acid-tolerant  $[\text{Ni}(1,4,8,11\text{-tetraazacyclotetradecane})]^{2+}$  catalyst achieves  $>30\%$   $\text{CO}$  selectivity at  $100 \text{ mA cm}^{-2}$  in a zero-gap r-BPM device fed with pure water and  $\text{CO}_2$ .<sup>65</sup> Cobalt phthalocyanine (CoPc) achieved 53%  $\text{CO}$  selectivity at  $100 \text{ mA cm}^{-2}$  and an  $\text{SPC}$  up to 51%.<sup>66</sup> Cobalt tetraaminophthalocyanine covalently anchored on the positively charged polyfluorene backbone (PF-CoTAPc) achieves 82.6%  $\text{FE}_{\text{CO}}$  at  $100 \text{ mA cm}^{-2}$  and 87.8%  $\text{CO}_2$  utilization.<sup>67</sup> More efforts are needed to develop electrocatalysts with intrinsically high  $\text{eCO}_2\text{R}$  selectivity and stability in pure acid or water.

Nanostructured electrocatalysts have the benefit of reducing the current/area and modulating the concentration of reactants/intermediates/products. But the coexistence of  $\text{H}^+$ , adsorbates such as  $^*\text{CO}$  and negative bias in acidic  $\text{eCO}_2\text{R}$  MEAs generates highly corrosive conditions for the popular M–N–C, Cu and Ag based electrocatalysts, causing demetallation in M–N–C and migration of surface-active metal atoms, and deactivating these electrocatalysts.<sup>68,69</sup> We think the activity, selectivity, stability, and cost of the nanostructured electrocatalysts should all be taken into account and well-balanced. Constructing highly stable electrocatalysts, which are resilient to harsh conditions through strong metal–support interactions or surface polymer/carbon coating, may be able to alleviate the corrosion of electrocatalysts in acidic MEAs.

(2) Designing highly conductive and stable CPLs. CPLs play crucial roles in manipulating the  $\text{CO}_2$ ,  $\text{H}_2\text{O}$ ,  $\text{CO}_3^{2-}/\text{HCO}_3^-$  and  $\text{K}^+/\text{Cs}^+$  transportation in the triphasic gas–electrode–electrolyte interface.<sup>46</sup> CPLs with high ionic conductivity and microphase separation structure are expected to decouple the  $\text{CO}_2$  and ion transfer pathway and boost the  $\text{eCO}_2\text{R}$  kinetics.<sup>45</sup> Moreover,

more chemically and mechanically stable CPLs are highly desired to enhance the durability of acidic MEAs.

(3) Systematically engineering the cathode CL/membrane interface. For the conventional catalyst-coated substrate (CCS) method, the cathode CL/membrane ionic interface contributes the major voltage loss,<sup>70</sup> which hinders the energy efficiency and current density. Constructing novel micro-/nano-structures such as three-dimensional (3D) ordered CLs with interlocked catalyst/membrane interface should boost the ion transfer and elevate the energy efficiency.<sup>71</sup>

(4) Quantitatively understanding and optimizing acidic  $\text{eCO}_2\text{R}$  MEAs by numerical simulations. In contrast to the conventional try-and-error experimental approach, numerical simulations play a key role in the development of  $\text{eCO}_2\text{R}$  electrolyzers by providing a deep and quantitative understanding of the transportation behavior of reactants/intermediates/products and their local concentration at the electrode/electrolyte interface with less cost.<sup>72–77</sup> The insight gained from numerical simulation will provide useful guidance for developing selective and stable acidic  $\text{eCO}_2\text{R}$  MEAs.

(5) Operando characterizations and monitoring the chemical microenvironment and interface in acidic  $\text{eCO}_2\text{R}$  MEAs. Monitoring the chemical microenvironment and the interface during operando conditions is significant for unraveling the failure mechanism of acidic  $\text{eCO}_2\text{R}$  MEAs, but is still at the early stage. Developing more *in situ* and operando techniques such as synchrotron radiation X-ray absorption spectroscopy (XAS), Raman spectroscopy, operando X-ray diffraction (XRD), and electrochemical impedance spectroscopy (EIS) with distribution of relaxation times (DRT) analysis is highly suggested to reveal the electronic structure of catalysts, evolution of the intermediates and local pH, salt precipitation and water flooding in GDEs, and changes in the catalyst/membrane interface.<sup>78–81</sup>

## Author contributions

Q. B., L. X., Y. Z., M. M. and Z. J.: writing – original draft and editing, investigation, visualization, data curation. Y. P., Z. D. and F. L.: conceptualization, resources, supervision, methodology, writing – review and editing, funding acquisition.

## Data availability

No primary research results, software or code have been included and no new data were generated or analysed as part of this review.

## Conflicts of interest

There are no conflicts to declare.



## Acknowledgements

This work is supported by the National Natural Science Foundation of China (No. 22309125, 22072101, 22075193, 22109099), the Natural Science Foundation of Jiangsu Province (No. BK20220483, BK20211306, BK20220027, BK20221239), the Natural Science Foundation of the Jiangsu Higher Education Institutions of China (22KJB150010), Six Talent Peaks Project in Jiangsu Province (No. TD-XCL-006), Chen Guang project from Shanghai Municipal Education Commission and Shanghai Education Development Foundation, and the Priority Academic Program Development (PAPD) of Jiangsu Higher Education Institutions.

## Notes and references

- 1 S. M. Jordaan and C. Wang, *Nat. Catal.*, 2021, **4**, 915–920.
- 2 C. Chen, H. Jin, P. Wang, X. Sun, M. Jaroniec, Y. Zheng and S.-Z. Qiao, *Chem. Soc. Rev.*, 2024, **53**, 2022–2055.
- 3 C. Tang, Y. Zheng, M. Jaroniec and S.-Z. Qiao, *Angew. Chem., Int. Ed.*, 2021, **60**, 19572–19590.
- 4 Z. Zhang, X. Huang, Z. Chen, J. Zhu, B. Endrődi, C. Janáky and D. Deng, *Angew. Chem., Int. Ed.*, 2023, **62**, e202302789.
- 5 C. Yan, D. Gao, J.-J. Velasco-Vélez and G. Wang, *EES Catal.*, 2024, **2**, 220–230.
- 6 C. A. Giron Rodriguez, N. C. Kani, A. B. Moss, B. O. Joensen, S. Garg, W. Deng, T. Wilson, J. R. Varcoe, I. Chorkendorff and B. Seger, *EES Catal.*, 2024, **2**, 850–861.
- 7 E. F. Johnson, E. Boutin, S. Liu and S. Haussener, *EES Catal.*, 2023, **1**, 704–719.
- 8 S. Kwon, T.-H. Kong, N. Park, P. Thangavel, H. Lee, S. Shin, J. Cha and Y. Kwon, *EES Catal.*, 2024, **2**, 911–922.
- 9 T. Burdyny and W. A. Smith, *Energy Environ. Sci.*, 2019, **12**, 1442–1453.
- 10 Z. Yin, H. Peng, X. Wei, H. Zhou, J. Gong, M. Huai, L. Xiao, G. Wang, J. Lu and L. Zhuang, *Energy Environ. Sci.*, 2019, **12**, 2455–2462.
- 11 J. Han, B. Tu, P. An, J. Zhang, Z. Yan, X. Zhang, C. Long, Y. Zhu, Y. Yuan, X. Qiu, Z. Yang, X. Huang, S. Yan and Z. Tang, *Adv. Mater.*, 2024, e2313926.
- 12 J. A. Rabinowitz and M. W. Kanan, *Nat. Commun.*, 2020, **11**, 5231.
- 13 J. E. Huang, F. Li, A. Ozden, A. S. Rasouli, F. P. G. D. Arquer, S. Liu, S. Zhang, M. Luo, X. Wang, Y. Lum, Y. Xu, K. Bertens, R. K. Miao, C.-T. Dinh, D. Sinton and E. H. Sargent, *Science*, 2021, **372**, 1074–1078.
- 14 N. McQueen, K. V. Gomes, C. McCormick, K. Blumanthal, M. Pisciotta and J. Wilcox, *Prog. Energy*, 2021, **3**, 032001.
- 15 K. V. Petrov, C. I. Koopman, S. Subramanian, M. T. M. Koper, T. Burdyny and D. A. Vermaas, *Nat. Energy*, 2024, **9**, 932–938.
- 16 C. P. O'Brien, R. K. Miao, S. Liu, Y. Xu, G. Lee, A. Robb, J. E. Huang, K. Xie, K. Bertens, C. M. Gabardo, J. P. Edwards, C.-T. Dinh, E. H. Sargent and D. Sinton, *ACS Energy Lett.*, 2021, **6**, 2952–2959.
- 17 H. Shin, K. U. Hansen and F. Jiao, *Nat. Sustainability*, 2021, **4**, 911–919.
- 18 B. Pan, J. Fan, J. Zhang, Y. Luo, C. Shen, C. Wang, Y. Wang and Y. Li, *ACS Energy Lett.*, 2022, **7**, 4224–4231.
- 19 S. C. da Cunha and J. Resasco, *Nat. Commun.*, 2023, **14**, 5513.
- 20 A. Ozden, F. P. García de Arquer, J. E. Huang, J. Wicks, J. Sisler, R. K. Miao, C. P. O'Brien, G. Lee, X. Wang, A. H. Ip, E. H. Sargent and D. Sinton, *Nat. Sustainability*, 2022, **5**, 563–573.
- 21 J. R. Varcoe, P. Atanassov, D. R. Dekel, A. M. Herring, M. A. Hickner, P. A. Kohl, A. R. Kucernak, W. E. Mustain, K. Nijmeijer, K. Scott, T. Xu and L. Zhuang, *Energy Environ. Sci.*, 2014, **7**, 3135–3191.
- 22 X. Tian, P. Zhao and W. Sheng, *Adv. Mater.*, 2019, **31**, 1808066.
- 23 Y. Y. Birdja, E. Pérez-Gallent, M. C. Figueiredo, A. J. Göttle, F. Calle-Vallejo and M. T. M. Koper, *Nat. Energy*, 2019, **4**, 732–745.
- 24 S. Feng, X. Wang, D. Cheng, Y. Luo, M. Shen, J. Wang, W. Zhao, S. Fang, H. Zheng, L. Ji, X. Zhang, W. Xu, Y. Liang, P. Sautet and J. Zhu, *Angew. Chem., Int. Ed.*, 2024, **63**, e202317942.
- 25 M. C. O. Monteiro, F. Dattila, B. Hagedoorn, R. García-Muelas, N. López and M. T. M. Koper, *Nat. Catal.*, 2021, **4**, 654–662.
- 26 Y. Dong, M. Ma, Z. Jiao, S. Han, L. Xiong, Z. Deng and Y. Peng, *Chin. Chem. Lett.*, 2024, **35**, 109049.
- 27 J. Gu, S. Liu, W. Ni, W. Ren, S. Haussener and X. Hu, *Nat. Catal.*, 2022, **5**, 268–276.
- 28 C. J. Bondue, M. Graf, A. Goyal and M. T. M. Koper, *J. Am. Chem. Soc.*, 2021, **143**, 279–285.
- 29 S.-J. Shin, H. Choi, S. Ringe, D. H. Won, H.-S. Oh, D. H. Kim, T. Lee, D.-H. Nam, H. Kim and C. H. Choi, *Nat. Commun.*, 2022, **13**, 5482.
- 30 Z. Zhang, H. Li, Y. Shao, L. Gan, F. Kang, W. Duan, H. A. Hansen and J. Li, *Nat. Commun.*, 2024, **15**, 612.
- 31 G. P. Heim, M. A. Bruening, C. B. Musgrave, W. A. Goddard, J. C. Peters and T. Agapie, *Joule*, 2024, **8**, 1312–1321.
- 32 X. Yang, H. Ding, S. Li, S. Zheng, J.-F. Li and F. Pan, *J. Am. Chem. Soc.*, 2024, **146**, 5532–5542.
- 33 M. Sassenburg, M. Kelly, S. Subramanian, W. A. Smith and T. Burdyny, *ACS Energy Lett.*, 2023, **8**, 321–331.
- 34 A. Reyes, R. P. Jansonius, B. A. W. Mowbray, Y. Cao, D. G. Wheeler, J. Chau, D. J. Dvorak and C. P. Berlinguette, *ACS Energy Lett.*, 2020, **5**, 1612–1618.
- 35 D. Wakerley, S. Lamaison, J. Wicks, A. Clemens, J. Feaster, D. Corral, S. A. Jaffer, A. Sarkar, M. Fontecave, E. B. Duoss, S. Baker, E. H. Sargent, T. F. Jaramillo and C. Hahn, *Nat. Energy*, 2022, **7**, 130–143.
- 36 H.-G. Qin, F.-Z. Li, Y.-F. Du, L.-F. Yang, H. Wang, Y.-Y. Bai, M. Lin and J. Gu, *ACS Catal.*, 2023, **13**, 916–926.
- 37 S. Kato, S. Ito, S. Nakahata, R. Kurihara, T. Harada, S. Nakanishi and K. Kamiya, *ChemSusChem*, 2024, e202401013.
- 38 J. Disch, S. Ingenhoven and S. Vierrath, *Adv. Energy Mater.*, 2023, **13**, 2301614.



39 S. Weng, W. L. Toh and Y. Surendranath, *J. Am. Chem. Soc.*, 2023, **145**, 16787–16795.

40 M. Fan, J. E. Huang, R. K. Miao, Y. Mao, P. Ou, F. Li, X.-Y. Li, Y. Cao, Z. Zhang, J. Zhang, Y. Yan, A. Ozden, W. Ni, Y. Wang, Y. Zhao, Z. Chen, B. Khatir, C. P. O'Brien, Y. Xu, Y. C. Xiao, G. I. N. Waterhouse, K. Golovin, Z. Wang, E. H. Sargent and D. Sinton, *Nat. Catal.*, 2023, **6**, 763–772.

41 D. Song, Y. Lian, M. Wang, Y. Su, F. Lyu, Z. Deng and Y. Peng, *eScience*, 2023, **3**, 100097.

42 J. Fan, B. Pan, J. Wu, C. Shao, Z. Wen, Y. Yan, Y. Wang and Y. Li, *Angew. Chem., Int. Ed.*, 2024, **63**, e202317828.

43 S. Favero, I. E. L. Stephens and M.-M. Titirci, *Adv. Mater.*, 2024, **36**, 2308238.

44 S. Garg, C. A. Giron Rodriguez, T. E. Rufford, J. R. Varcoe and B. Seger, *Energy Environ. Sci.*, 2022, **15**, 4440–4469.

45 D. A. Salvatore, C. M. Gabardo, A. Reyes, C. P. O'Brien, S. Holdcroft, P. Pintauro, B. Bahar, M. Hickner, C. Bae, D. Sinton, E. H. Sargent and C. P. Berlinguette, *Nat. Energy*, 2021, **6**, 339–348.

46 E. W. Lees, B. A. W. Mowbray, F. G. L. Parlante and C. P. Berlinguette, *Nat. Rev. Mater.*, 2022, **7**, 55–64.

47 H.-G. Qin, Y.-F. Du, Y.-Y. Bai, F.-Z. Li, X. Yue, H. Wang, J.-Z. Peng and J. Gu, *Nat. Commun.*, 2023, **14**, 5640.

48 X. She, L. Zhai, Y. Wang, P. Xiong, M. M.-J. Li, T.-S. Wu, M. C. Wong, X. Guo, Z. Xu, H. Li, H. Xu, Y. Zhu, S. C. E. Tsang and S. P. Lau, *Nat. Energy*, 2024, **9**, 81–91.

49 M. Hefselmann, J. K. Lee, S. Chae, A. Tricker, R. G. Keller, M. Wessling, J. Su, D. Kushner, A. Z. Weber and X. Peng, *ACS Appl. Mater. Interfaces*, 2024, **16**, 24649–24659.

50 L. Xue, Z. Gao, T. Ning, W. Li, J. Li, J. Yin, L. Xiao, G. Wang and L. Zhuang, *Angew. Chem., Int. Ed.*, 2023, **62**, e202309519.

51 M. Zhusansun, Y. Liu, R. Lu, F. Zeng, Z. Xu, Y. Wang, Y. Yang, Z. Wang, G. Zheng and Y. Wang, *Angew. Chem., Int. Ed.*, 2023, **62**, e202309875.

52 W. Li, Z. Yin, Z. Gao, G. Wang, Z. Li, F. Wei, X. Wei, H. Peng, X. Hu, L. Xiao, J. Lu and L. Zhuang, *Nat. Energy*, 2022, **7**, 835–843.

53 Q. Xu, A. Xu, S. Garg, A. B. Moss, I. Chorkendorff, T. Bligaard and B. Seger, *Angew. Chem., Int. Ed.*, 2023, **62**, e202214383.

54 J. C. Bui, E. W. Lees, L. M. Pant, I. V. Zenyuk, A. T. Bell and A. Z. Weber, *Chem. Rev.*, 2022, **122**, 11022–11084.

55 Y. C. Tan, K. B. Lee, H. Song and J. Oh, *Joule*, 2020, **4**, 1104–1120.

56 L.-C. Weng, A. T. Bell and A. Z. Weber, *Phys. Chem. Chem. Phys.*, 2018, **20**, 16973–16984.

57 H. Li, H. Li, P. Wei, Y. Wang, Y. Zang, D. Gao, G. Wang and X. Bao, *Energy Environ. Sci.*, 2023, **16**, 1502–1510.

58 T. Alkayyali, A. S. Zeraati, H. Mar, F. Arabyarmohammadi, S. Saber, R. K. Miao, C. P. O'Brien, H. Liu, Z. Xie, G. Wang, E. H. Sargent, N. Zhao and D. Sinton, *ACS Energy Lett.*, 2023, **8**, 4674–4683.

59 M. Wang, L. Lin, Z. Zheng, Z. Jiao, W. Hua, G. Wang, X. Ke, Y. Lian, F. Lyu, J. Zhong, Z. Deng and Y. Peng, *Energy Environ. Sci.*, 2023, **16**, 4423–4431.

60 Q. Wen, S. Pan, Y. Li, C. Bai, M. Shen, H. Jin, F. Ning, X. Fu and X. Zhou, *ACS Energy Lett.*, 2022, **7**, 3900–3909.

61 M. Sun, J. Cheng and M. Yamauchi, *Nat. Commun.*, 2024, **15**, 491.

62 B. Endrődi, E. Kecsenovity, A. Samu, F. Darvas, R. V. Jones, V. Török, A. Danyi and C. Janáky, *ACS Energy Lett.*, 2019, **4**, 1770–1777.

63 B. Endrődi, A. Samu, E. Kecsenovity, T. Halmágyi, D. Sebők and C. Janáky, *Nat. Energy*, 2021, **6**, 439–448.

64 A. T. Chu, O. Jung, W. L. Toh and Y. Surendranath, *J. Am. Chem. Soc.*, 2023, **145**, 9617–9623.

65 B. Siritanaratkul, M. Förster, F. Greenwell, P. K. Sharma, E. H. Yu and A. J. Cowan, *J. Am. Chem. Soc.*, 2022, **144**, 7551–7556.

66 B. Siritanaratkul, P. K. Sharma, E. H. Yu and A. J. Cowan, *Adv. Mater. Interfaces*, 2023, **10**, 2300203.

67 G. Li, L. Huang, C. Wei, H. Shen, Y. Liu, Q. Zhang, J. Su, Y. Song, W. Guo, X. Cao, B. Z. Tang, M. Robert and R. Ye, *Angew. Chem., Int. Ed.*, 2024, **63**, e202400414.

68 Y. Yang, S. Louisia, S. Yu, J. Jin, I. Roh, C. Chen, M. V. Fonseca Guzman, J. Feijóo, P.-C. Chen, H. Wang, C. J. Pollock, X. Huang, Y.-T. Shao, C. Wang, D. A. Muller, H. D. Abruña and P. Yang, *Nature*, 2023, **614**, 262–269.

69 X. Li, P. Zhang, L. Zhang, G. Zhang, H. Gao, Z. Pang, J. Yu, C. Pei, T. Wang and J. Gong, *Chem. Sci.*, 2023, **14**, 5602–5607.

70 K. U. Hansen, L. H. Cherniack and F. Jiao, *ACS Energy Lett.*, 2022, **7**, 4504–4511.

71 L. Wan, J. Liu, D. Lin, Z. Xu, Y. Zhen, M. Pang, Q. Xu and B. Wang, *Energy Environ. Sci.*, 2024, **17**, 3396–3408.

72 L.-C. Weng, A. T. Bell and A. Z. Weber, *Energy Environ. Sci.*, 2019, **12**, 1950–1968.

73 L.-C. Weng, A. T. Bell and A. Z. Weber, *Energy Environ. Sci.*, 2020, **13**, 3592–3606.

74 N. Gupta, M. Gattrell and B. MacDougall, *J. Appl. Electrochem.*, 2006, **36**, 161–172.

75 Y. Lum, B. Yue, P. Lobaccaro, A. T. Bell and J. W. Ager, *J. Phys. Chem. C*, 2017, **121**, 14191–14203.

76 Y. Xie, P. Ou, X. Wang, Z. Xu, Y. C. Li, Z. Wang, J. E. Huang, J. Wicks, C. McCallum, N. Wang, Y. Wang, T. Chen, B. T. W. Lo, D. Sinton, J. C. Yu, Y. Wang and E. H. Sargent, *Nat. Catal.*, 2022, **5**, 564–570.

77 C.-T. Dinh, T. Burdyny, M. G. Kibria, A. Seifitokaldani, C. M. Gabardo, F. P. G. D. Arquer, A. Kiani, J. P. Edwards, P. D. Luna, O. S. Bushuyev, C. Zou, R. Quintero-Bermudez, Y. Pang, D. Sinton and E. H. Sargent, *Science*, 2018, **360**, 783–787.

78 S. Brückner, Q. Feng, W. Ju, D. Galliani, A. Testolin, M. Klingenhof, S. Ott and P. Strasser, *Nat. Chem. Eng.*, 2024, **1**, 229–239.

79 B. O. Joensen, J. A. Zamora Zeledon, L. Trotochaud, A. Sartori, M. Mirolo, A. B. Moss, S. Garg, I. Chorkendorff, J. Drnec, B. Seger and Q. Xu, *Joule*, 2024, **8**, 1754–1771.

80 A. B. Moss, S. Garg, M. Mirolo, C. A. Giron Rodriguez, R. Ilvonen, I. Chorkendorff, J. Drnec and B. Seger, *Joule*, 2023, **7**, 350–365.

81 Y. Qu, K. Yang, W. Li, G. Wang, L. Xiao, G. Wang and L. Zhuang, *ACS Energy Lett.*, 2024, **9**, 3042–3048.

